**ORIGINAL ARTICLE**

# Effects of primary sintering on microstructure and properties of friction stir back extruded Cu–Ti$_2$SnC wire composite

Amirhossein Jahani[1] · Hamed Jamshidi Aval[1] · Mohammad Rajabi[1] · Roohollah Jamaati[1]

**Abstract**

The present work investigated the effects of primary sintering on the microstructure, mechanical, electrical, and wear properties of the Cu–5vol%Ti$_2$SnC wire composite fabricated by friction stir back extrusion process. The results showed that the grain size of the final product increased by performing a sintering treatment before the FSBE process. It is important to note that the grain size in the composite sample was coarser than the sample without reinforcement after the extrusion process. Furthermore, since the effect of temperature predominates over plastic strain, a coarser grain was formed in the composite samples. Compared to the center, the grain size of the near surface of extruded wires was slightly finer. By performing the sintering treatment and applying heat during the treatment, it is possible to form the Cu$_{81}$Sn$_{22}$ phase, which can increase the Cu$_{81}$Sn$_{22}$ phase content formed during FSBE. The interface quality was significantly improved by the sintering treatment before the FSBE process. The sintering treatment increased the strength, elongation, electrical conductivity, and wear resistance of Cu–Ti$_2$SnC composite wire by 4, 13, 2, and 5%, respectively.

**Keywords** Friction stir back extrusion · Cu–Ti$_2$SnC composite · Primary sintering · Mechanical properties · Wear resistance

## 1 Introduction

Pure copper, with its high thermal and electrical conductivity, is used in many industrial applications, especially in electrical applications like high-performance electric switches and sliding contact materials [1]. However, copper has a low hardness and wear resistance, which limits its use in many engineering applications [2]. One potential solution to this problem is fabricating copper matrix composite [3]. Considering the rapid development of industries and advanced technologies, it is essential to use a new reinforcement to improve the properties of the copper matrix [4]. A family of new materials called the MAX phase has a combination of metallic and ceramic properties. The MAX phases, ternary carbides, and nitrides have hexagonal structures with the general formula $M_{n+1}AX_n$, in which $M$ is an early transition metal, $A$ is an element from columns 13 to

16 in the periodic table, $X$ is C or N, and $n = 1$–3 [5]. The MAX phases have good electrical and thermal conductivity, machinability, high-temperature strength, corrosion resistance and high elastic moduli, low density, self-lubrication properties, and quasi-plasticity characteristics [6]. Ti$_2$SnC as a MAX phase has good machinability, high strength, a low friction coefficient, and good self-lubrication properties with a hardness of 3.5 GPa ± 0.4 GPa and a density of 6.1 g cm$^{-3}$. Ti$_2$SnC, between more than 155 MAX phases, shows the highest electrical conductivity ($14 \times 10^6$ $\Omega^{-1}$ m$^{-1}$) and can be used to strengthen the copper matrix composite [7].

Copper matrix composites can be produced either in the liquid or solid state [8]. Many production processes can be carried out with the liquid state method, but the main disadvantage is the high reactivity of melt/reinforcement [9]. The friction stir back extrusion (FSBE) is a novel thermomechanical and solid-state method based on the friction stir process and extrusion [10]. It is a new sustainable manufacturing process that can produce fine-grained wire or tubular shapes [11]. In this process, powder, chips, bars, or any other feedstock can be extruded and turned into a defect-free final product in one step without melting [12]. Depending on the type of precursor used in this process, the FSBE process can

✉ Hamed Jamshidi Aval
   h.jamshidi@nit.ac.ir

1  Department of Materials Engineering, Babol
   Noshirvani University of Technology, Shariati Avenue,
   Babol 47148-71167, Iran

also be used to fabricate metal matrix composites. Numerous researchers have reported wire fabrication by the FSBE process [13]. However, only a few studies have been conducted to investigate the fabrication of copper matrix composites.

Li et al. [14] recently studied the fabrication of copper–carbon composite wire using the FSBE method. They reported that the carbon powder was refined to a sub-micron level and uniformly dispersed in the copper matrix. Compared with pure copper, the thermal capacity of the composite wire increased by 30% while its density decreased by 29%. Recently, Jahani et al. [15] studied the effect of $Ti_2SnC$ content on the microstructure, mechanical, electrical, and wear properties of friction stir back extrusion (FSBE)-processed $Cu–Ti_2SnC$ composite wire. They found that by increasing the content of the $Ti_2SnC$ phase, the hardness of the composite increased and reached 280.51 HV for a composite containing 30 vol.% $Ti_2SnC$ phases. In addition, the highest electrical conductivity (95.67% IASC) was obtained in a composite containing 1 vol% $Ti_2SnC$ phases.

The literature indicates that $Ti_2SnC$ as a MAX phase exhibits the highest electrical conductivity and a high Young's modulus among MAX phases. Conversely, severe plastic deformation and heat generation during FSBE can result in unique properties in the final product. Therefore, in order to take advantage of the unique properties of the $Ti_2SnC$ phase and the advantages of the FSBE process, in this research, a $Cu–Ti_2SnC$ composite was made by the FSBE process. The fabrication of copper matrix composites has been studied using the FSBE process in previous research; however, the effect of the processing performed before the FSBE process on the properties of the final product has not been explored. This study investigated the effects of the sintering step performed prior to the FSBE process on the prototype. To do this, first, $Cu–5vol\%Ti_2SnC$ composites were prefabricated using powder metallurgy, then the effect of performing sintering treatment on prototype $Cu–5vol\%Ti_2SnC$ composites was examined. The FSBE process was performed at rotational and extrusion speeds. Afterward, the microstructure, mechanical, electrical, and tribological properties of the composite wires were characterized.

## 2 Experimental procedure

This research used copper powder (minimum purity of 99.9%) as a matrix and $Ti_2SnC$ powder (minimum purity of 99.9%) as composite reinforcement. Figure 1 shows the scanning electron microscope (SEM) image of copper powder and the MAX phase. Copper powder and $Ti_2SnC$ powder with average particle sizes of 5 μm and 15 μm were used, respectively. For fabrication of $Cu–5vol\%Ti_2SnC$ prototype composite, the copper powder with the constant value of $5vol\%Ti_2SnC$ were mixed. Powders were ball milled in Ball Mill PM 100 at a rotation speed of 300 rpm for 10 min using a steel ball with an average diameter of 10 mm. Ar gas was used as the protective atmosphere during the milling.

Then, the mixed powder was cold pressed in a die, and a cylindrical prototype composite with 20 mm diameter and 30 mm length was prepared. In order to investigate sintering treatment, one of the cold-pressed prototype composites was sintered in an electrical furnace under the protection of Ar
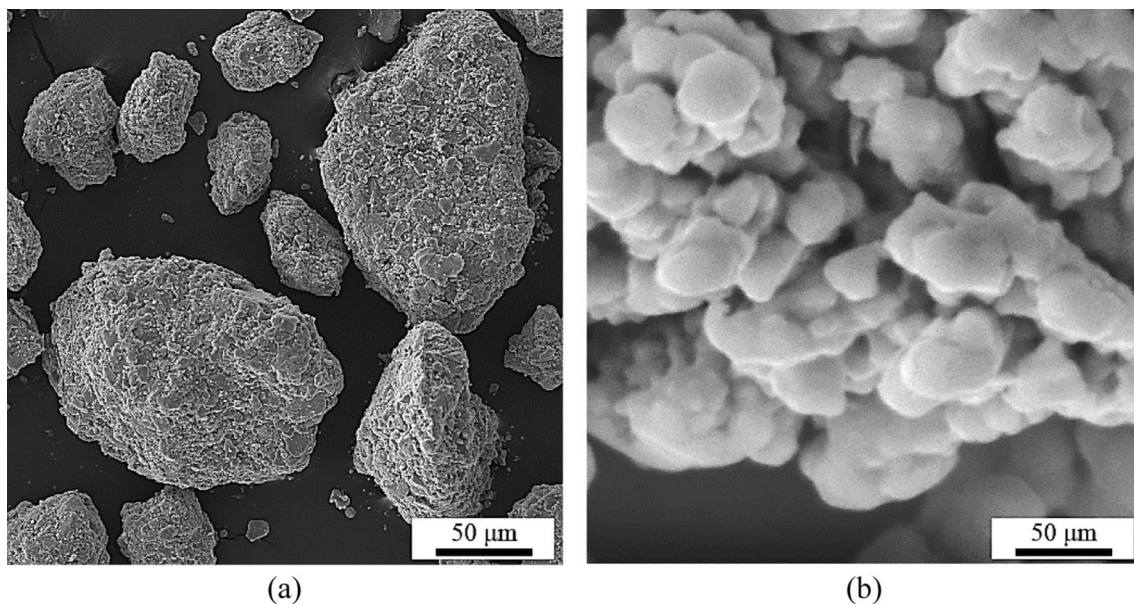


(a)

(b)

**Fig. 1** SEM image of: **a** $Ti_2SnC$ powder, and **b** copper powder

gas for 30 min at 850 °C. Meanwhile, the other sample was subjected to FSBE without sintering treatment. The FSBE process was performed on both samples at a constant rotational speed of 600 rpm and an extrusion speed of 85 mm/min. The die and punch of the FSBE process were fabricated from H13 steel. Figure 2 illustrates the dimensions of the die and punch. Different samples of FSBE-processed in this study are labeled according to Table 1. In naming different samples, S and G indicate whether or not the prototype underwent a sintering treatment before the extrusion process. In addition, C and W denote composite wire with and without reinforcement, respectively. Moreover, number 85 specifies the extrusion speed in mm/min; for instance, SC-85 is the designation for composite wire whose prototype is sintered prior to FSBE.

A scanning electron microscope (Philips-XL30FSEM) with an EDS detector and an optical microscope (NGF-120A optical microscope) was used to examine the microstructural evolution. At the same time, a Rigaku Ultima IV X-ray diffraction instrument was employed to determine the phases. The microstructure of the metallographic samples was examined using a cross-section made using SiC sandpaper and a suspension of alumina. Afterward, the cross-section of the samples was etched to reveal the microstructure using a solution of 85 ml distilled water, 15 ml HCl, and 5 g $FeCl_3$. The hardness of the samples in Vickers scale was measured using a Koopa Universal (UV1) microhardness tester with a load of 100 gr at an interval of 15 s. A microhardness test was conducted under the ASTM E384 standard. The tensile test was performed using the SANTAM-STM250 tensile test machine with a crosshead speed of 1 mm/min. In addition, the wires' tribological and electrical properties were evaluated using the pin-on-disc test according to standard ASTM G99 and the electrical conductivity test according to ASTM B63 standard, respectively. The wear test was performed using the pin-on-disc method. The counterface was made of

**Table 1** The FSBE-processed sample labeling

| Sample label | Rotational speed (rpm) | Traverse speed (mm/min) | Reinforcement | Sintering of prototype |
|---|---|---|---|---|
| Sample GW-85 | 600 | 85 | – | – |
| Sample SW-85 | 600 | 85 | – | Done |
| Sample GC-85 | 600 | 85 | $Ti_2SnC$ | – |
| Sample SC-85 | 600 | 85 | $Ti_2SnC$ | Done |

steel with a hardness of 60 HRC. The wear test was carried out under a load of 20 N at a distance of 2000 m. After the tensile and wear test, the fracture and wear surfaces of the samples were examined by SEM.

## 3 Results and discussion

Figure 3 shows optical microscope images of the cross-section of different samples. The images contain two parts: the left part relates to the center, and the right part relates to the near surface of the sample. Figure 3a, b demonstrates optical microscope images of the prototype composites, including before and after sintering. Figure 4 shows the grain size of different samples. The average grain sizes of $2.8 \pm 0.6$ μm and $3.6 \pm 0.9$ μm relate to the before and after sintering composite, respectively. As seen in two of these samples, there is no difference between the grain size in the center and the near surface of prototype composites. Figure 3c–f shows the microstructure of the FSBE-processed samples. Since the FSBE process is inherently thermo-mechanical, recrystallized grains can be formed in the structure under

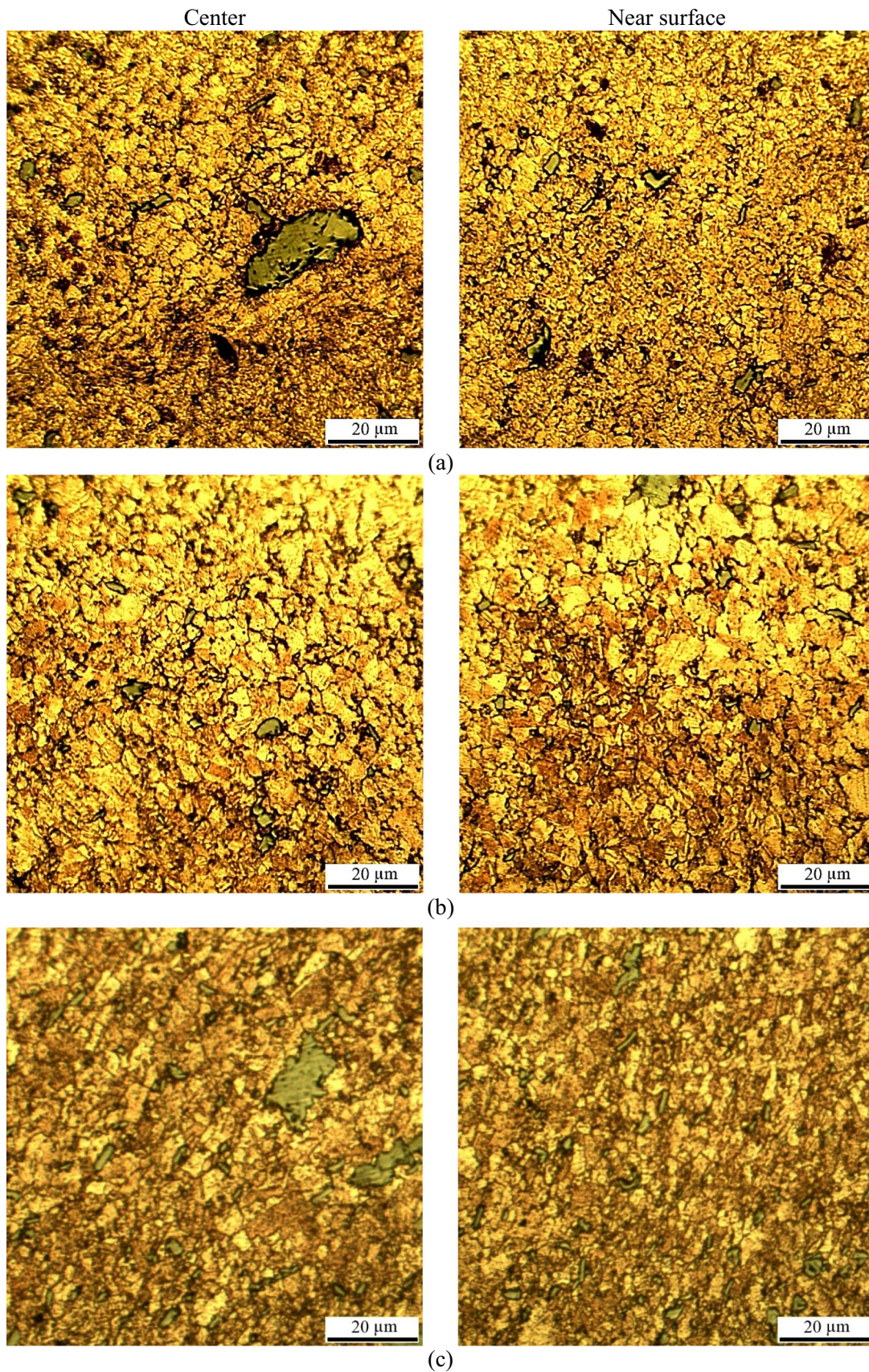**Fig. 2** The dimension of: **a** die and **b** punch used in the FSBE process



(a)                    (b)

Center          Near surface
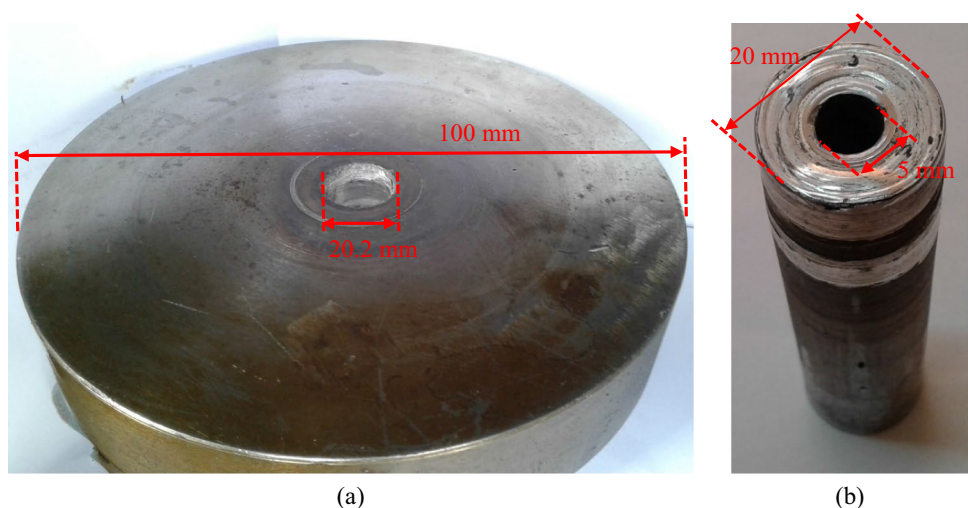


Fig. 3 Optical microscopy image of microstructure of: **a** Cu–Ti$_2$SnC composite before sintering, **b** Cu–Ti$_2$SnC composite after sintering, **c** sample GC-85, **d** sample SC-85, **e** sample GW-85, **f** sample SW-85
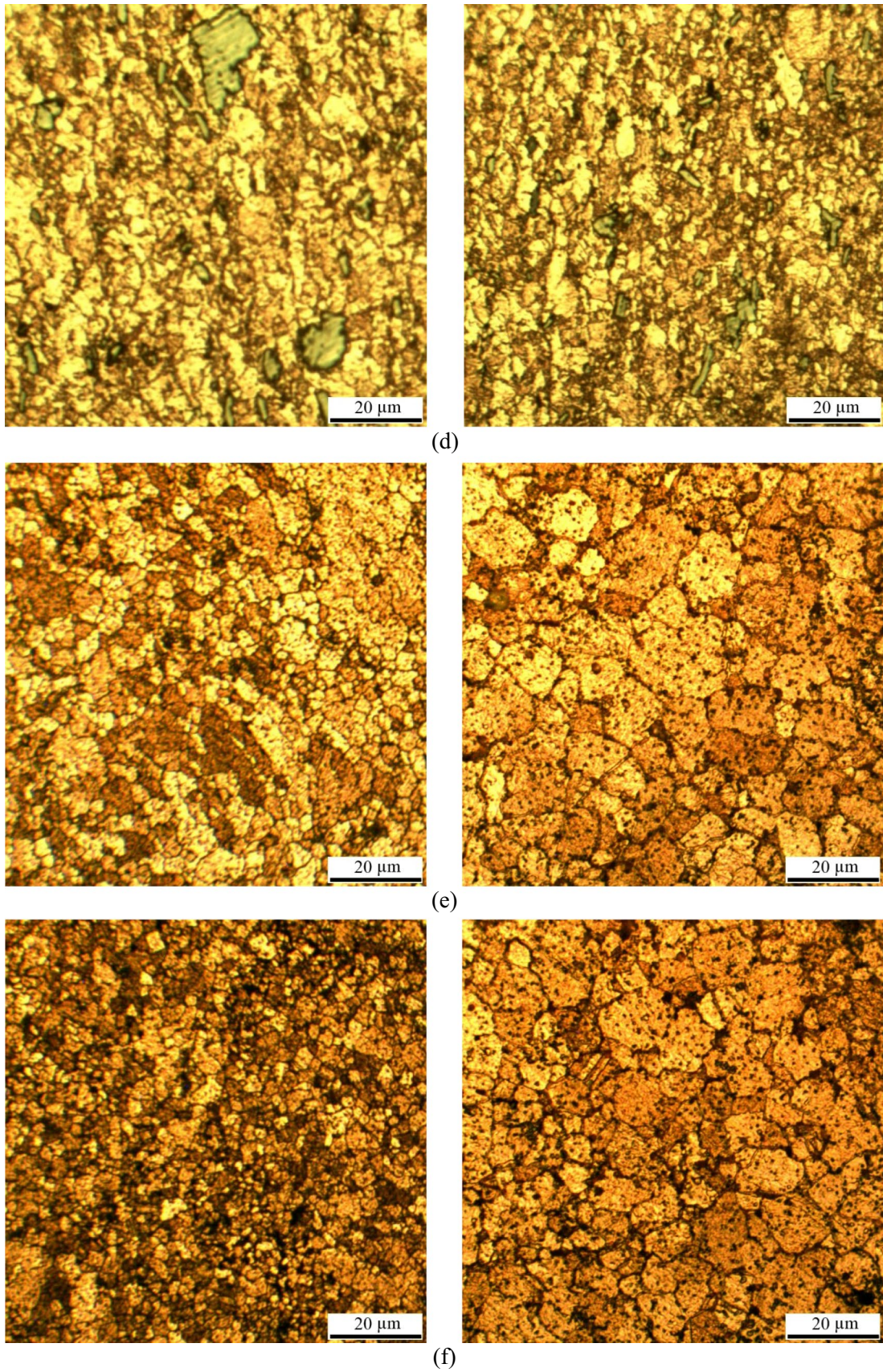
(d)
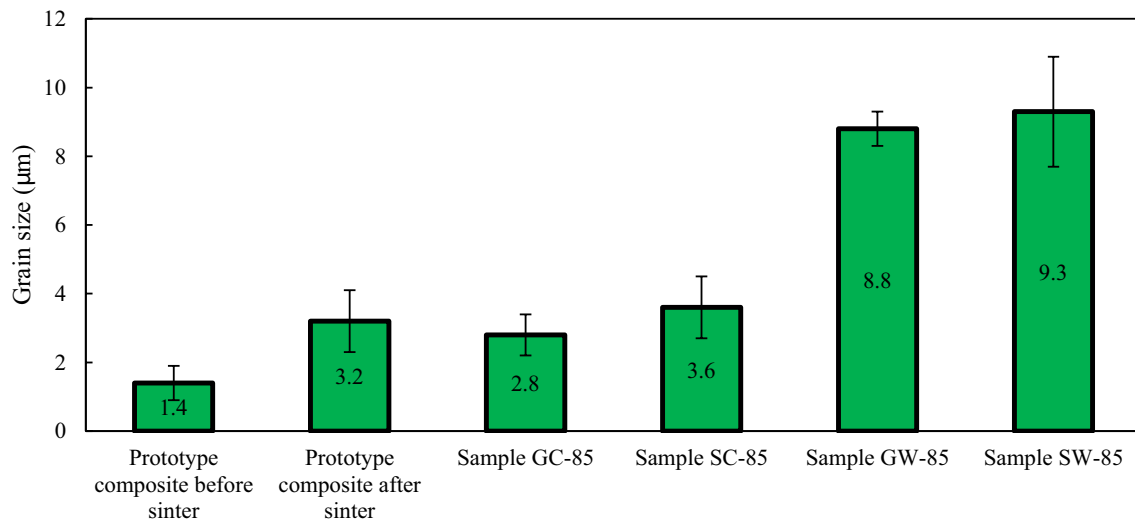
(e)

(f)

**Fig. 3** (continued)

**Fig. 4** Average grain size of different samples

the influence of heat and plastic deformation. Different factors have a role in determining recrystallized grain size but thermal history and the plastic strain play the most dominant roles in the microstructure in the FSBE process [16]. It was reported that grain size increased as the maximum temperature increased and plastic strain decreased. The reverse trend in the grain size was observed when the maximum temperature decreased and the plastic strain increased. The grain size of the samples GC-85, SC-85, GW-85, and SW-85 is $2.8 \pm 0.6$, $3.6 \pm 0.9$, $8.8 \pm 0.5$, and $9.3 \pm 1.6$ μm, respectively. The grain size of the samples GC-85 and SC-85 is coarser than their primary composites. This phenomenon indicates that under the influence of applied heat during the FSBE process, the grains in the prototype have grown in size, and grain size has increased as a result. Furthermore, sintering before FSBE leads to coarser grain sizes after wire extrusion. Therefore, it can be concluded that increasing initial grain size in prototype (by sintering treatment) increases grain size after extrusion.

The same trend is observed in the extruded samples without reinforcement (GW-85 and SW-85). In other words, by performing a sintering treatment before the FSBE process, the grain size of the final product increases. Notably, the grain size in the composite sample is coarser than the sample without reinforcement after the extrusion process. According to [17], adding $Ti_2SnC$ reinforcements increases the amount of heat generated during the FSBE process. On the other hand, due to the presence of reinforcing particles, the amount of plastic strain decreases. Therefore, since the effect of temperature predominates over the effect of plastic strain, coarser grains are formed in the composite samples. Comparing two prototype composite samples before the extrusion process revealed that the copper grain size grew

after sintering. Copper matrix particles underwent sintering, but despite the change in porosity of the copper matrix, the interface between the particles and the copper matrix did not change much, and no proper bond was formed between them. It is evident that after the extrusion process, most of the particles were broken under the influence of the applied strain. In addition, most pores and discontinuities between the particles and the matrix disappeared.

In composite wires, the broken $Ti_2SnC$ caused by the FSBE process facilitates the nucleation of more sites for recrystallization and acts as a barrier to grain growth [18]. Nevertheless, as seen in Figs. 3 and 4, the grain size of the pure copper wires is smaller than the composite wire. It should be noted that more plastic strain in the pure copper wires provides more sites for recrystallization. Another factor that contributes to smaller grain sizes is the cooling rate. Since pure copper has higher thermal conductivity and a lower maximum temperature during processing than Cu–$Ti_2SnC$ composites, the un-reinforced wires present a higher cooling rate than reinforced copper. Compared to the center, the grain size of the near surface of extruded wires is slightly finer. Although the near surface of the extruded wires endures higher strain and a bit higher temperature, the effect of strain overcomes the temperature effect and produces finer grains [19].

Figure 5 shows the phase analysis of the different samples investigated by XRD. The first peak of copper in all extruded wires shifts to a higher angle, suggesting the generation of compressive stress produced by the FSBE process (Fig. 5). The diffraction patterns of Cu and $Ti_2SnC$ were observed in all composite samples. Furthermore, the heat and plastic deformation generated during FSBE caused some of the tin in the MAX phase to diffuse
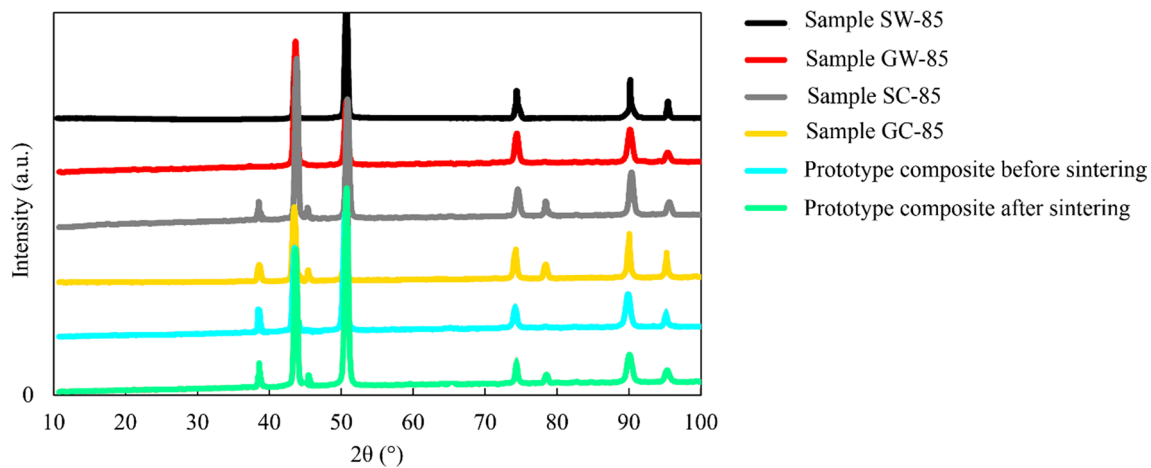
**Fig. 5** X-ray diffraction pattern of different samples

toward the copper matrix, and the $Cu_{81}Sn_{22}$ mixture was formed in the composite samples. The $Cu_{81}Sn_{22}$ phase content obtained from the method of the intensity ratio of diffraction peaks for samples GC-85 and SC-85 shows values of 0.41 and 0.54, respectively. These results show that in addition to the difference in microstructure in these two samples, the $Cu_{81}Sn_{22}$ phase content is different, and the sintering process significantly changes the $Cu_{81}Sn_{22}$ phase content. In fact, when the sintering treatment is performed and heat is applied during the process, it is possible to form the $Cu_{81}Sn_{22}$ phase, which would increase the $Cu_{81}Sn_{22}$ phase content formed during FSBE.

To quantitatively estimate the lattice reorientation, a texture parameter ($TP_{hkl}$) of various samples was calculated per the method described in [20], utilizing $I_{hkl}$ (measured integrated intensity of plane $\{hkl\}$) and $R_{hkl}$ (calculated integrated intensity of plane $\{hkl\}$ in a completely random arrangement of crystals) for numerous diffraction peaks (denoted here by $n$). The texture parameter (($TP_{hkl}$) is defined as

$$TP_{hkl} = \frac{I_{hkl}/R_{hkl}}{\frac{1}{n}\sum_0^n \left(I_{hkl}/R_{hkl}\right)}, \tag{1}$$

where $I_{hkl}$ denotes the intensity of $\{hkl\}$ in primary composite samples and extruded wires, while $R_{hkl}$ represents the intensity of $\{hkl\}$ in copper with random orientation. The symbol $\{\}$ represents the set of equivalent planes.

For example, the sample GC-85 texture parameter is calculated as follows: as previously stated, $I_{hkl}$ is the intensity of $\{hkl\}$ in the primary composite samples and extruded wires. In sample GC-85, the intensity of the first peak at an angle of 43.3° ($I_{111}$) is 100%, the second peak at an angle of 50.4° ($I_{200}$) is 43.32%, the third peak at an angle of 74.0° ($I_{220}$) is 12.54%, and the fourth peak at an angle of 89.9° ($I_{311}$) is

18.32%. Furthermore, $R_{hkl}$ is the intensity of $\{hkl\}$ in the copper with random orientation.

The JCPDS reference code 00-004-0836 was used for $R_{hkl}$ values. As per the JCPDS reference code 00-004-0836, the first peak ($I_{111}$) has an intensity of 100%, the second peak ($I_{200}$) has an intensity of 46%, the third peak ($I_{220}$) has an intensity of 20%, and the fourth peak ($I_{311}$) has an intensity of 17%. At this point, because the fraction's denominator is constant across all crystallographic planes, the denominator is calculated using Eq. (1).

The intensity of four peaks in the sample GC-85 ($I_{hkl}$) is divided by the intensity of four related peaks in the reference code 00–004-0836 ($R_{hkl}$), where the values for the first to fourth peaks are 1.00, 0.94, 0.63, and 1.07, respectively. This value is 0.73 when the sum of the results is divided by the number of peaks (4). Finally, the texture parameter corresponding to each crystallographic plane is calculated using Eq. (1).

As evident from Table 2, adding the MAX phase and adjusting the sintering conditions of the prototype sample does not significantly alter the texture parameter. However, it should be noted that a change in the texture parameter occurs. Thus, the FSBE process may create a weak texture in

**Table 2** The texture parameters of different samples

| Sample label | (111) | (200) | (220) | (311) |
|---|---|---|---|---|
| Prototype composite before sinter | 1.26 | 1.17 | 0.53 | 0.62 |
| Prototype composite after sinter | 1.15 | 1.03 | 0.73 | 0.91 |
| Sample GC-85 | 1.08 | 0.98 | 0.75 | 0.88 |
| Sample SC-85 | 1.30 | 1.14 | 0.57 | 0.75 |
| Sample GW-85 | 1.23 | 1.17 | 0.63 | 0.82 |
| Sample SW-85 | 1.38 | 1.01 | 0.62 | 0.73 |

different samples based on the change in the texture parameter of different crystal plates.

Poor interfacial bonding can destroy the copper matrix composite's mechanical and physical properties. On the other hand, proper interfacial bonding decreases the content of the porosity [21]. Figure 6 shows the SEM images of the prototype composites before and after sintering and samples GC-85 and SC-85. In addition, Table 3 shows the

energy-dispersive spectroscopy (EDS) spot analysis of different zones marked in the Fig. 6. By performing the sintering treatment on prototype, the amount of porosity and deboned area in the interface (marked by yellow arrow) is greatly reduced. The interface quality is significantly improved by the sintering treatment before the FSBE process. Images demonstrated that the sintering treatment forms a significant amount of the $Cu_{81}Sn_{22}$ phase at the interface.
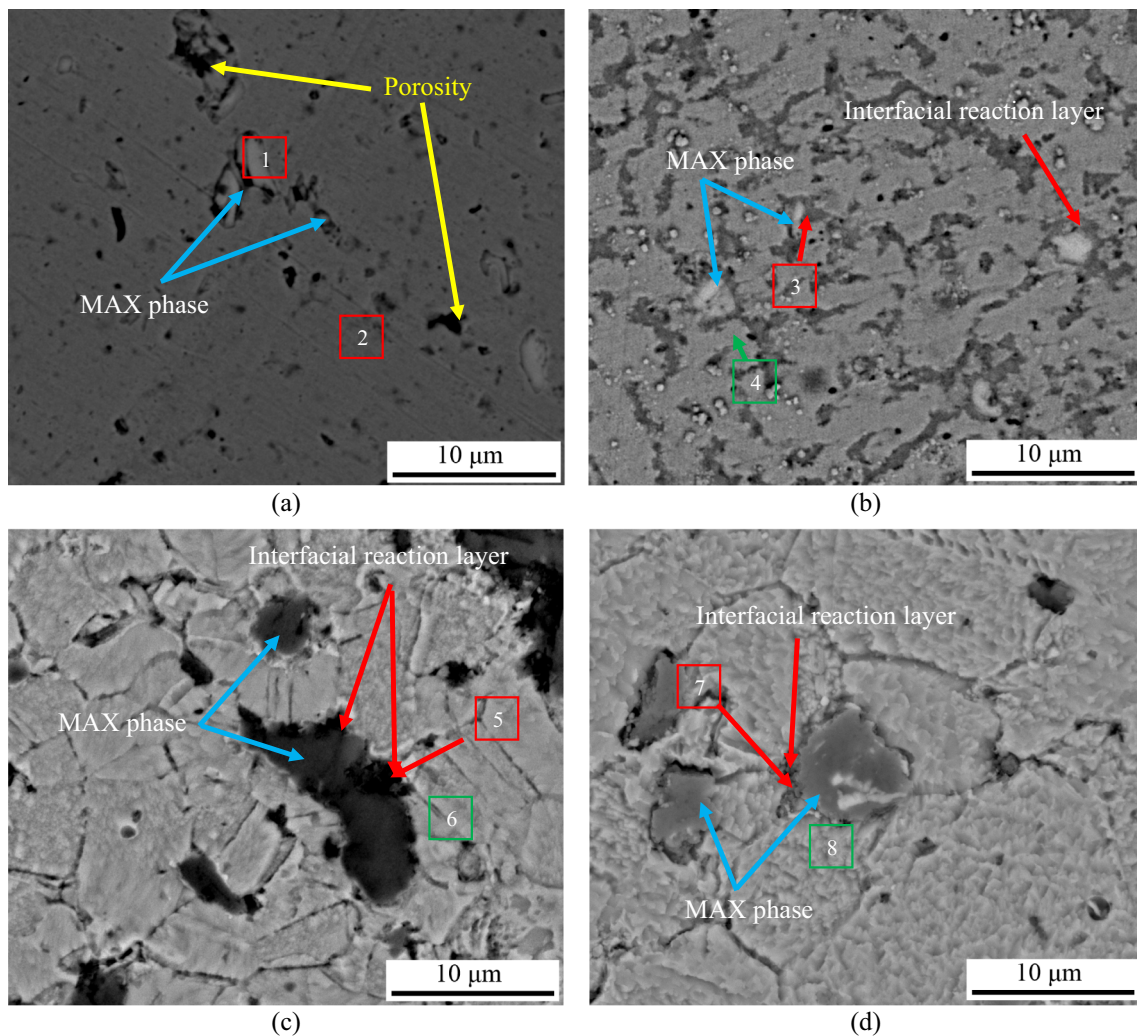


**Fig. 6** SEM micrograph of: **a** prototype composite before sintering, **b** prototype composite after sintering, **c** sample GC-85, **d** sample SC-85 (the porosity, MAX phase, and interfacial reaction layer marked by yellow, blue, and red arrows, respectively)

**Table 3** Chemical composition of different points marked in Fig. 6 (at.% means atomic percent)

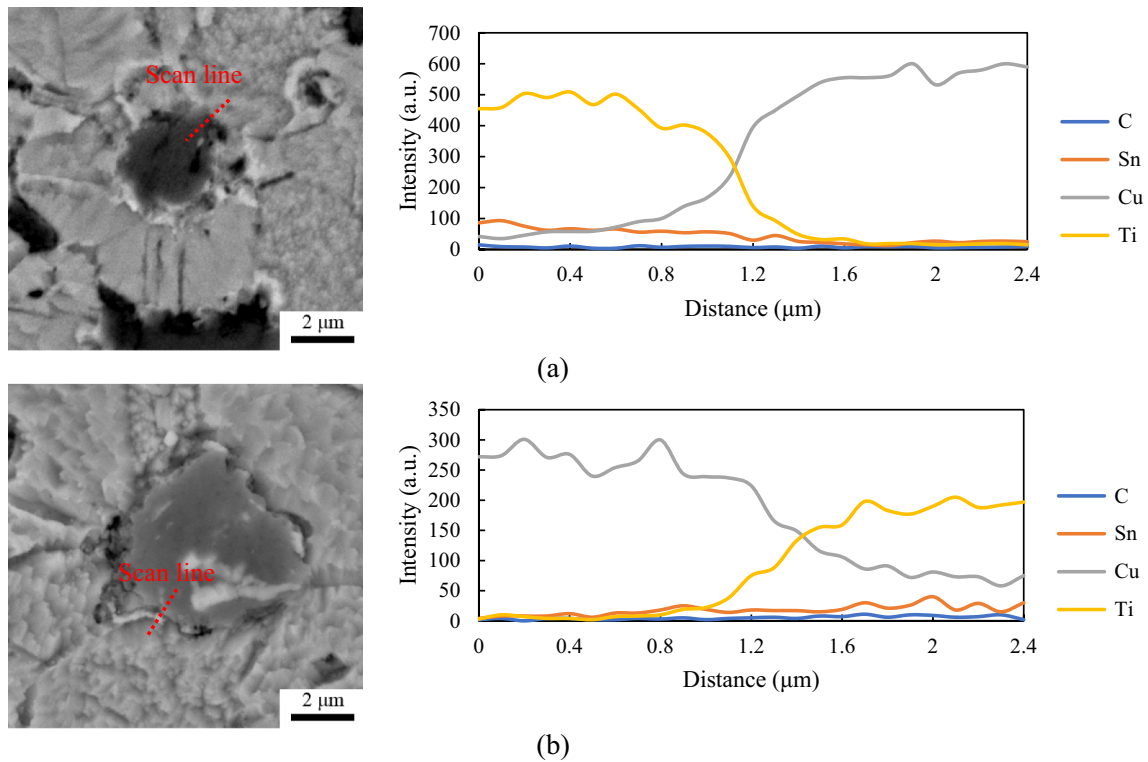| Chemical element | Marking in Fig. 6 | | | | | | | |
|---|---|---|---|---|---|---|---|---|
| | 1 | 2 | 3 | 4 | 5 | 6 | 7 | 8 |
| Ti (at.%) | 54.23 | 0.45 | 0.45 | 1.23 | 0.89 | 1.09 | 0.67 | 0.89 |
| Sn (at.%) | 23.11 | 0.19 | 15.23 | 0.98 | 17.13 | 0.54 | 19.02 | 0.67 |
| C (at.%) | 22.34 | 0.10 | 0.13 | 0.34 | 0.34 | 0.32 | 0.09 | 0.23 |
| Cu (at.%) | 0.32 | 99.26 | 84.19 | 97.45 | 81.64 | 98.05 | 80.22 | 98.21 |

**Fig. 7** SEM image of interface and corresponding EDS line scan of: **a** sample GC-85, **b** sample SC-85

Although after the FSBE processing, most of these integrated $Cu_{81}Sn_{22}$ phases are broken, they increase the amount of the $Cu_{81}Sn_{22}$ phase in the copper matrix. Figure 7 shows the SEM image, including the EDX line scan analysis of SC-85 and GC-85. The high temperature during the FSBE process can accelerate the reaction of the alloying elements and make the formation of intermetallic phases easy [22]. The element distribution curve indicates that there has been an interdiffusion between Cu and Sn. The interdiffusion

**Table 4** The maximum temperature and plastic strain of different samples

| Sample label | Maximum temperature (°C) | Plastic strain (mm/mm) |
|---|---|---|
| Sample GW-85 | $744 \pm 1$ | $36.1 \pm 0.3$ |
| Sample SW-85 | $776 \pm 3$ | $39.6 \pm 0.4$ |
| Sample GC-85 | $735 \pm 2$ | $35.1 \pm 0.3$ |
| Sample SC-85 | $764 \pm 4$ | $37.9 \pm 0.6$ |

**Fig. 8** The probability density function for the distribution of the nearest particles
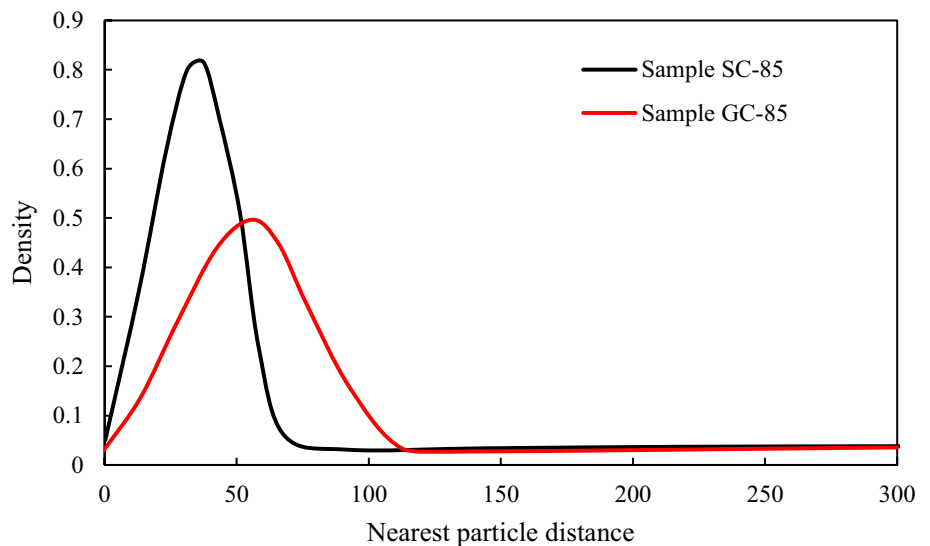
between Cu and Sn strengthens the bonding between the matrix and reinforcement. The Cu(Sn) and TiC$_x$ are reacting products controlled by Sn decomposition from Ti$_2$SnC. A close relationship exists between the reacting products and the temperature of the reaction. Therefore, SC-85 exhibits accelerated reaction rates and increased content of reacting products resulting from the higher temperature (according to Table 4 maximum temperatures during FSBE of sample GC-85 and SC-85 were $735 \pm 2$ and $764 \pm 4$ °C, respectively). Accordingly, the integrated bond is formed at the interface.

The diagram of the distribution of reinforcing particles in samples GC-85 and SC-85 was obtained and reported in Fig. 8 to analyze the distribution of reinforcing particles after the FSBE process, according to the method proposed in [17]. By performing the sintering treatment, the distribution of reinforcing particles becomes more uniform, and the average size of the particles decreases. While the difference between the two samples is not very substantial, perhaps the more uniform distribution in sample SC-85 can be attributed to the composite's initial strength. In fact, increasing the strength of the bond between the particle and the matrix in the prototype creates greater stress in the interface during the FSBE process, which can help fracture the particles and disperse them more evenly in the copper matrix.
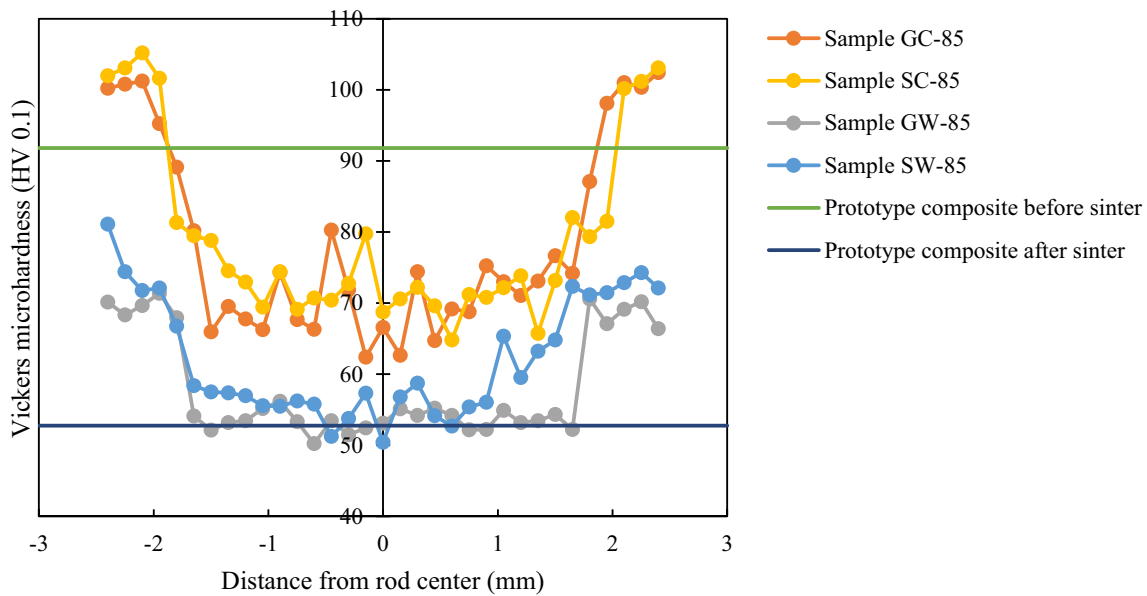


(a)
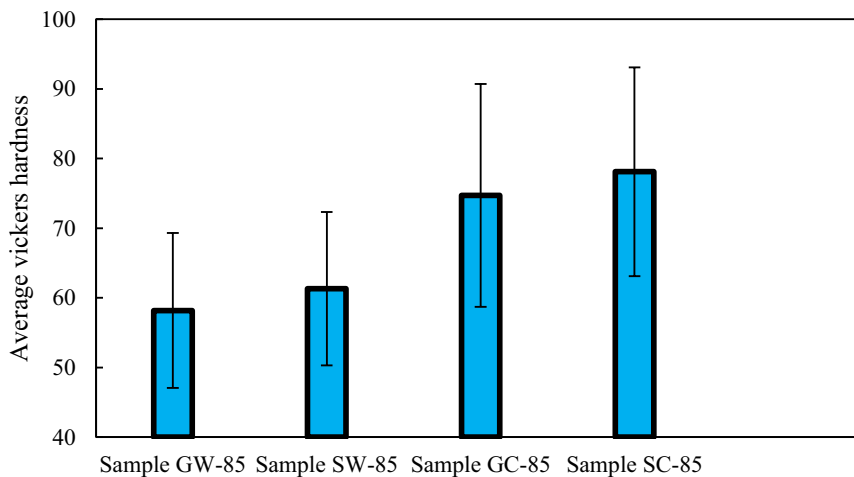


(b)

**Fig. 9** **a** Vickers microhardness profile and **b** average hardness of different samples

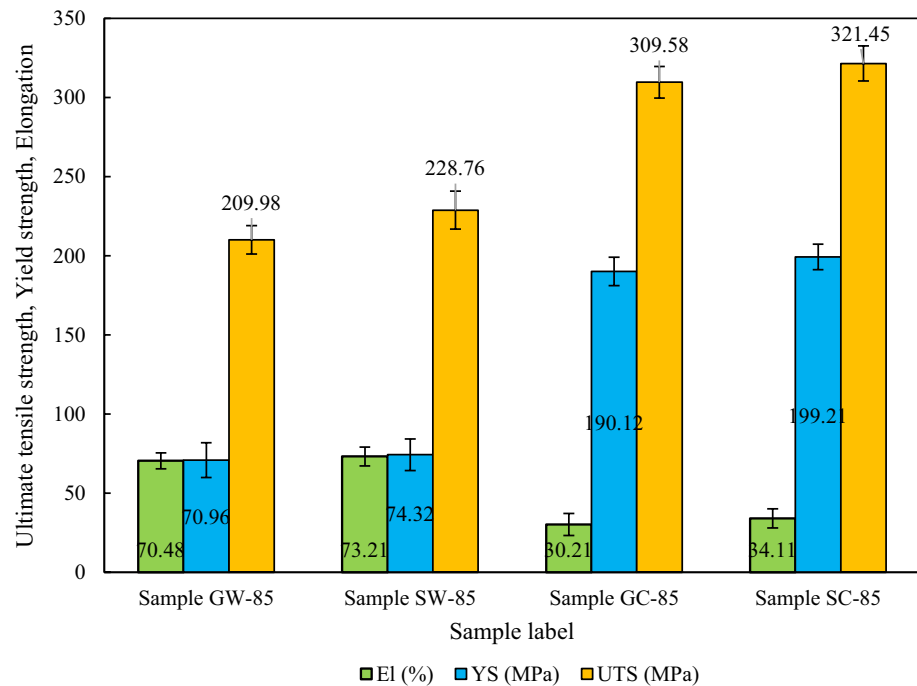**Fig. 10** The tensile test property of different samples



Figure 9 shows the microhardness profile of different samples. The hardness value of the prototype composites before sintering is higher than after sintering. This phenomenon can be related to finer grains and strain induced during cold pressing of prototype composites before sintering. Performing the FSBE process causes non-uniformity in the hardness profile. The hardness of the extruded wires near the surface is higher than the center. In the FSBE process samples, noticeable grain changes are observed in these two areas; however, in the extrusion process, plastic strain is greater along the edge regions of the wire than in the central regions.

Moreover, the increase in the density of dislocations and residual stress in the edge regions can effectively increase the hardness in the edge regions of the wire compared to the central regions of the wire. The average hardness of samples GW-85, SW-85, GC-85, and SC-85 is $58.18 \pm 11.13$, $61.32 \pm 10.91$, $74.72 \pm 16.10$, and $78.11 \pm 15.21$ HV, respectively. The sintering process results in a more uniform distribution of reinforcing particles, a reduction of particle size, and an improvement of bond quality at the interface, which leads to a higher average hardness for the sintered sample (sample SC-85) compared to the composite sample without sintering (sample GC-85). Similarly, although the grain size of sample GW-85 is smaller than sample SW-85, the hardness value increases due to greater cohesion in the copper matrix and reduced porosity.

The tensile test properties of different samples are presented in Fig. 10. The yield strength of samples GW-85, SW-85, GC-85, and SC-85 is $70.96 \pm 11.03$, $74.32 \pm 10.01$, $190.12 \pm 9.56$, and $199.21 \pm 8.56$ MPa, respectively. In addition, the ultimate tensile strength of samples GW-85, SW-85, GC-85, and SC-85 is $209.98 \pm 9.54$, $228.76 \pm 12.03$, $309.58 \pm 10.23$, and $321.45 \pm 11.45$ MP, respectively. The elongation of samples GW-85, SW-85, GC-85, and SC-85 is $70.48 \pm 5.21$, $73.21 \pm 6.20$, $30.21 \pm 7.45$, and $34.11 \pm 6.12\%$, respectively. As can be seen, in both reinforced and un-reinforced wires, the strength of samples increased by performing the sintering treatment. Besides, the sintering treatment can improve the elongation of samples. As discussed in the hardness result section, it is possible to improve the strength and ductility of sintered samples by enhancing the uniform distribution of reinforcing particles, reducing particle size, and improving the bond quality at the interface between composite wires, as well as greater cohesion in the copper matrix and reduced porosity in the un-reinforced wires. Several mechanisms may be effective in strengthening copper matrix composites, including grain refinement, solid solution strengthening, Orowan strengthening, the dislocation formed by the misfit of the thermal expansion coefficient, and load transfer strengthening [23].

Comparing the grain size of the composite wires to prototype composites demonstrated no grain size reduction for both composite wires (samples GC-85 and SC-85). As a result, the grain refinement mechanism does not contribute to improving strength. The strength of sample GC-85 is lower than sample SC-85, despite its finer grain size. It should be noted that interfacial reaction products such as Cu(Sn) solid solution and TiCx accelerated at higher
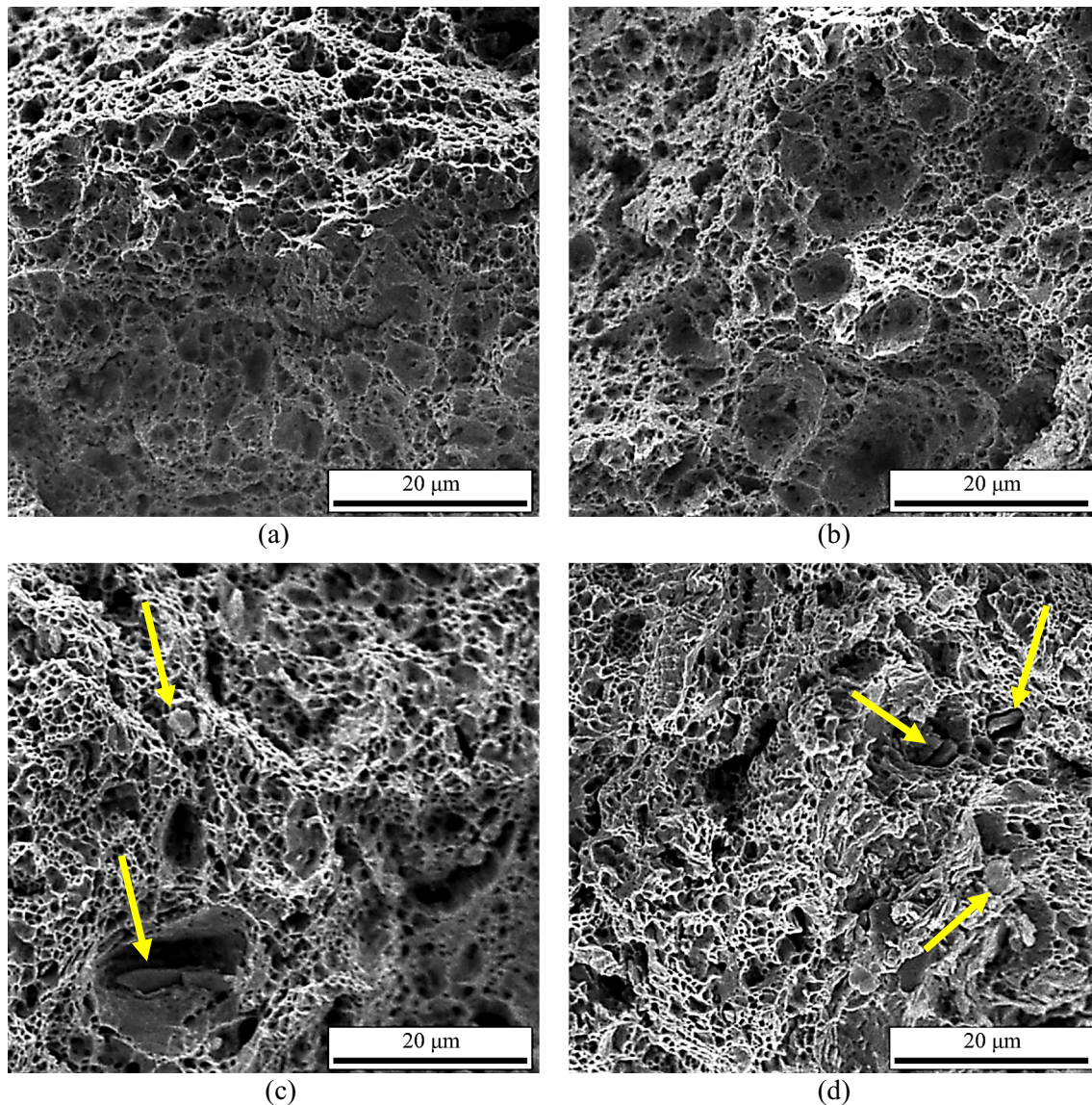
**Fig. 11** SEM image of fracture surface of: **a** sample GC-85, **b** sample SC-85, **c** sample GW-85, **d** sample SW-85 (the MAX phase marked by yellow arrows)

temperatures and time. As a result, the likelihood of forming these products is higher in sample SC-85 than in sample GC-85. Solid solution and dispersion strengthening mechanisms can improve mechanical properties by forming these products. Orowan strengthening is activated by fairly homogeneous reinforcement distribution [24]. The higher plastic strain at a higher temperature enables the sample SC-85 to form a more homogeneous distribution of reinforcement than the sample GC-85. Accordingly, the operation of the Orowan mechanism or the strength increment of this mechanism is higher in the sample SC-85. Finely dispersion of reinforcement between the grains plays a key role in Orowan strengthening. However, according to Figs. 3 and 6, this process has not happened properly, and the particles at the grain

boundaries do not effectively inhibit the movement of dislocations. Thus, this mechanism does not play a significant role in strengthening composite wires. The thermal mismatch of the matrix causes internal stresses, and reinforcement and dislocations can be formed in the matrix [25]. Since the reinforcement particles in the sample SC-85 are smaller and there is a higher thermal gradient, more dislocations can form, which results in a higher strength enhancement. Performance of the FSBE process can remove the porosity, particularly in Cu/Ti$_2$SnC interfacial part, shown in Fig. 6. Proper bonding occurs when the porosity is reduced, and interdiffusion activates the load transfer mechanism. As a result, it represents one of the major mechanisms of composite wires. In the un-reinforced samples, the higher strength

**Fig. 12** The electrical conductivity of different samples
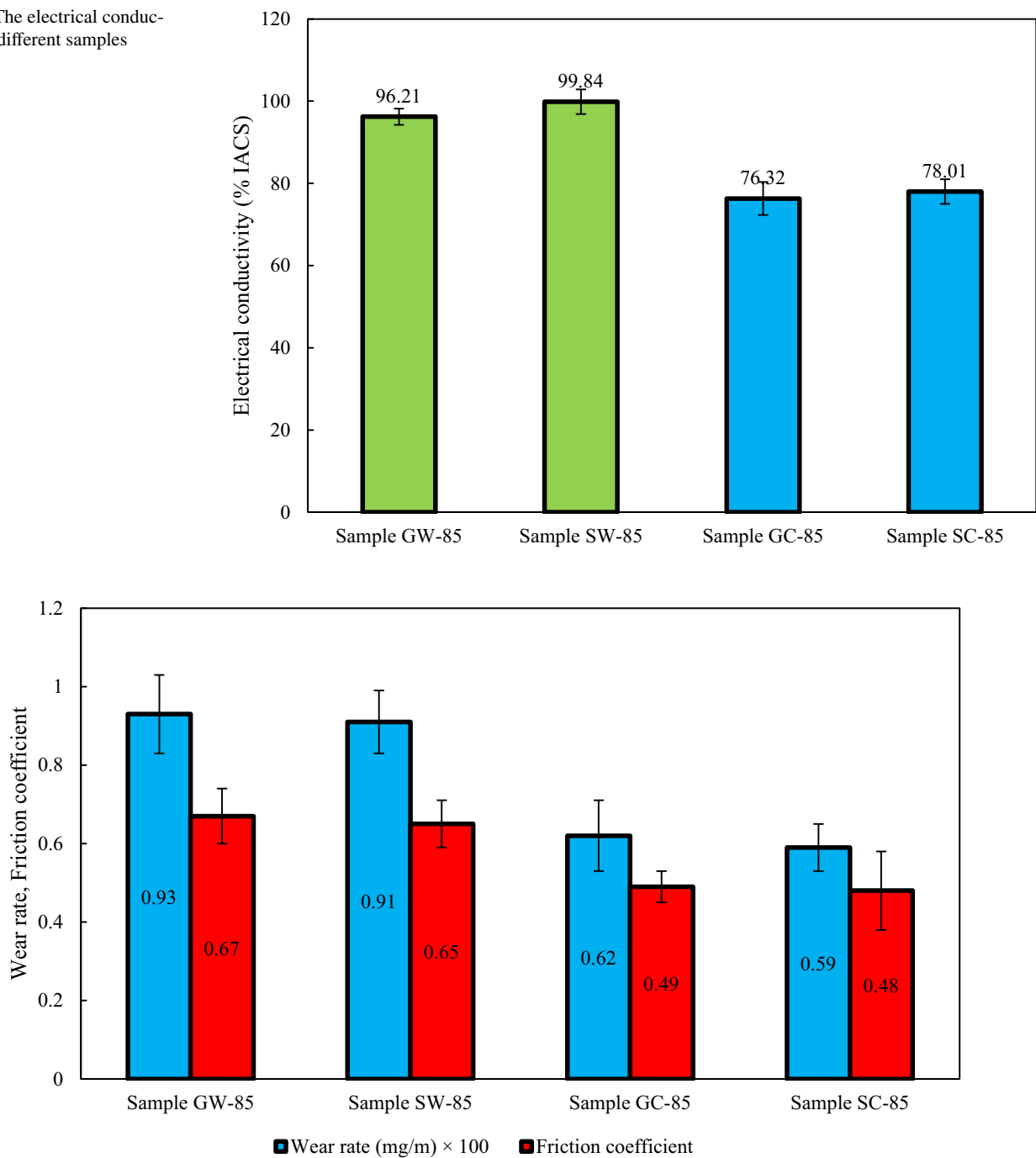


**Fig. 13** The wear rate and friction coefficient of different samples

of sample SW-85 compared to sample GW-85 can be related to lower porosity and more dislocations induced by higher plastic strain during the FSBE process in this sample.

Figure 11 shows SEM images related to the fracture surfaces of all extruded wires. Figure 11a, b illustrates the pure copper wires, and Fig. 11c, d relates to the composite wires. The dimples on the fracture surfaces of extruded wires indicate that the matrix tolerated significant plastic deformation prior to tensile failure, and thus it had a ductile nature. While pure copper wires have finer grains than composite wires, their dimples are not smaller due to the cavity coalescence. The reinforcement particles, however, in composite wires inhibit cracks from propagating as rapidly, resulting in higher tensile strength. The dimples on the fracture surface of the sample GC-85 are smaller and shallower due to lower plastic deformation and finer grains than the sample SC-85.
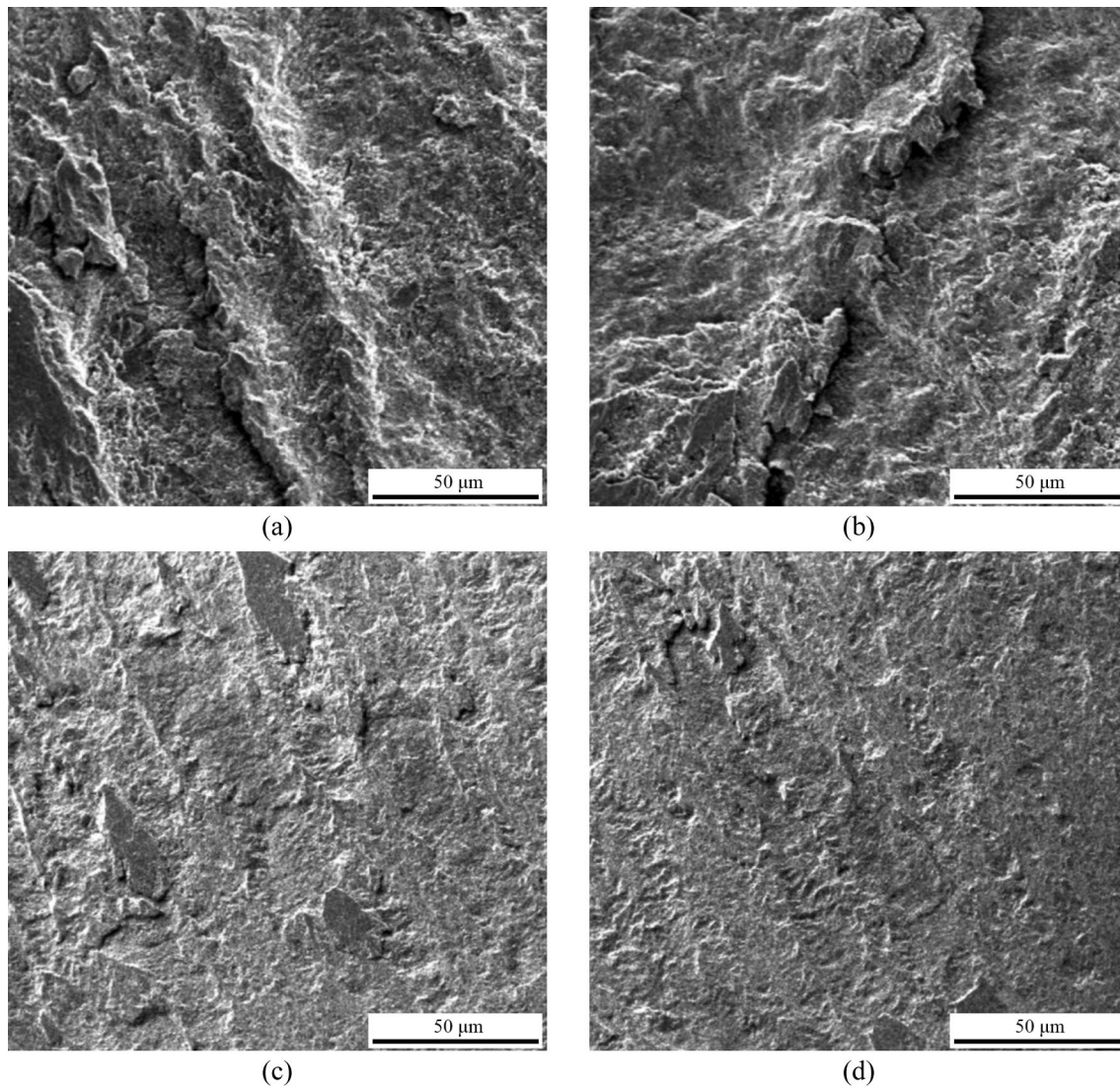
**Fig. 14** SEM image of worn surface of: **a** sample GC-85, **b** sample SC-85, **c** sample GW-85, **d** sample SW-85

In addition, the large voids in Fig. 11d show more elongation and ductile fracture than in Fig. 11c.

Figure 12 illustrates the electrical conductivity of pure copper wires and composite copper wires in terms of %IASC. The electrical conductivity of the samples GW-85 and SW-85 are $96.21 \pm 2.11$%IASC and $99.84 \pm 3.12$%IASC, respectively. The finer grain size of the sample GW-85 than the sample SW-85 causes more grain boundary resistivity [21]. The presence of more porosities in the sample GW-85 also contributes to the reduction in electrical conductivity. By adding the reinforcement, the electrical conductivity of the samples GC-85 and SC-85 reaches $76.32 \pm 4.21$%IASC and $78.01 \pm 3.43$%IASC, respectively. According to the rule of mixtures, the electrical conductivity of Cu–5vol%Ti$_2$SnC composite is predicted to be 86.96%IASC. The obtained electrical conductivity values for the composite wires are much less than the prediction. The main reason for this reduction is the electron scattering by dislocations, porosity, grain boundary, and scattering at the interface. The increased formation of Cu(Sn) and TiCx due to the higher temperature in sample SC-85 and finer grains in sample GC-86 is most likely the main causes of the electrical conductivity reduction. Finally, sample GC-85 has a lower electrical conductivity than sample SC-85, suggesting that the effect of porosities and fine grains in sample GC-85 is more dominant than the effect of more reaction products and dislocations in sample SC-85.

Figure 13 shows the wear rate and friction coefficient of the extruded wires. The average wear rate and friction coefficient of the sample GW-85 are $0.93 \pm 0.07$ and $0.67 \pm 0.10$, respectively, and for sample SW-85, they are $0.91 \pm 0.06$ and $0.65 \pm 0.08$, respectively. Adding Ti$_2$SnC improves
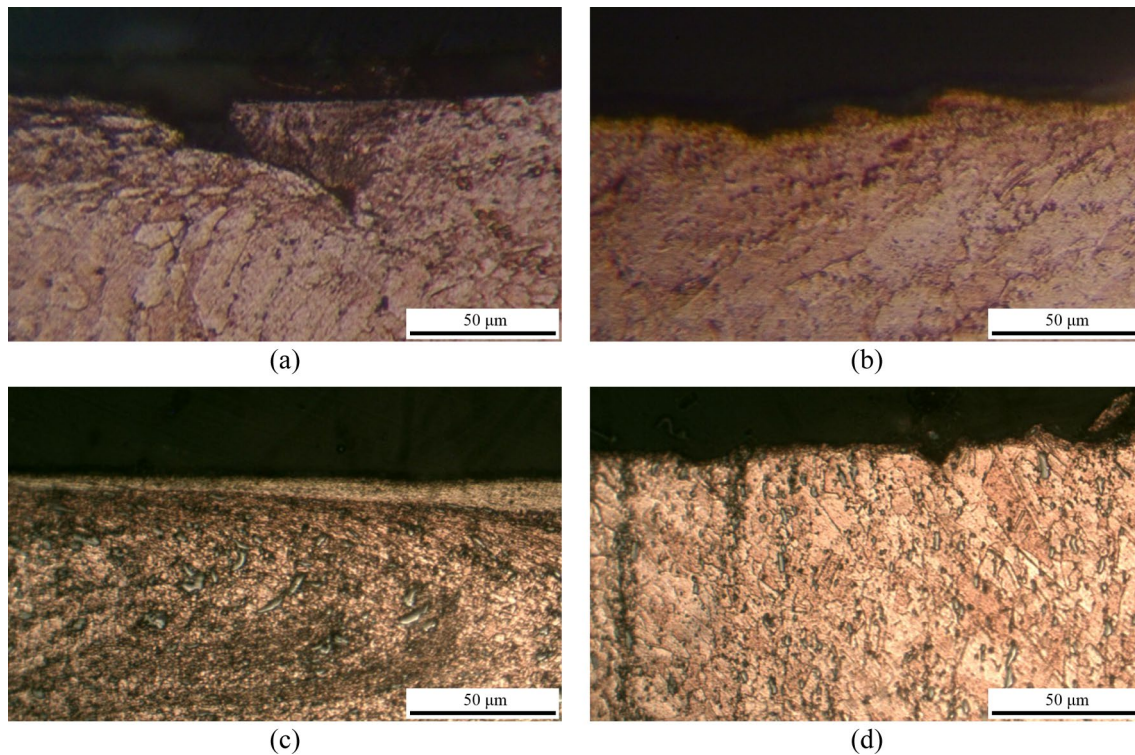
**Fig. 15** The cross-section of worn surface of: **a** sample GC-85, **b** sample SC-85, **c** sample GW-85, **d** sample SW-85

composite wire wear resistance due to its increased hardness and strength. In particular, the wear rate and friction coefficient are significantly reduced. In sample SC-85, the minimum wear rate and friction coefficient were $0.62 \pm 0.04$ and $0.49 \pm 0.09$, respectively. SEM images of the worn surface of different samples are shown in Fig. 14. As shown in Fig. 14a, b, the low hardness of the pure copper wires causes severe material removal at the surface, implying an adhesive wear mechanism. Although there is no significant difference in the wear surface of different un-reinforced samples (samples GW-85 and SW-85), by adding reinforcing particles, it is observed that the wear mechanism changes from adhesive to abrasive.

As shown in Fig. 15, increasing the hardness of samples decreases the wear scar's depth. Low hardness and surface plastic deformation are responsible for adhesion. The plough causes plastic deformation on the worn surface during the wear process. In composite wires, the wear mechanism changes from delamination to an abrasive mechanism by increasing surface hardness. By applying periodic pressure and shearing stress, wear debris retained at the friction interface is ground to a small particle size in the wear test of sample GC-85. Then, those little particle wear debris accumulates and interconnects with each other. Afterward, a mechanical mixture layer (MML) is formed on the worn surface due to sintering metallicity wear debris at high temperatures. This prevents a substantial increase in wear.

High temperatures also lead to the oxidation of MML. Parallel cracks easily produce oxidation defects in MML under periodic pressure and shear stress, causing delamination of MML. It is worth mentioning that once MML peels off, tiny particle wear debris is agglomerated again in the peeling pit, forming a new one.

## 4 Conclusion

This research investigated the effect of a sintering stage on the prototype before the FSBE process of Cu–5vol%Ti$_2$SnC composites. Then, the microstructure, mechanical, electrical, and tribological properties of the composite wires were characterized. The most important results include the following statements:

- Increasing the initial grain size in prototype (after sintering treatment) increased the grain size after extrusion. The same trend was observed in extruded samples without reinforcement.
- Under the influence of the plastic strain during the FSBE process, most of the Ti$_2$SnC particles were broken, and most of the pores and discontinuities between the particles and the copper matrix disappeared.

- While the near surface of extruded wires endured higher strain and a slightly higher temperature, strain dominated the temperature effect and produced finer grains.
- Performing the sintering treatment on prototype substantially reduced porosity and deboned area at the interface.
- By performing the sintering treatment, the distribution of reinforcing particles became more uniform, and the average size of the particles decreased.
- In both reinforced and un-reinforced wires, the strength of samples was increased by performing the sintering treatment. Besides, the sintering treatment can improve composite wire's elongation, electrical conductivity, and wear resistance by 13, 2, and 5%, respectively.
- In composite wires, the wear mechanism changes from delamination to an abrasive mechanism by increasing surface hardness.

## Declarations

**Conflict of interest** All the authors declare that they have no conflicts of interest.

**Ethical statement** The authors state that the research was conducted according to ethical standards.

## References

1. Avcu E, Cao H, Zhang X, Guo Y, Withers PJ, Li X, et al. The effect of reduced graphene oxide content on the microstructural and mechanical properties of copper metal matrix composites. Mater Sci Eng A. 2022;856: 143921.
2. Brillon A, Heintz J-M, Constantin L, Pillier F, Lu Y, Silvain J-F, et al. Anisotropic thermal conductivity and enhanced hardness of copper matrix composite reinforced with carbonized polydopamine. Compos Commun. 2022;33: 101210.
3. Yu W, Guénolé J, Ghanbaja J, Vallet M, Guitton A. Frank partial dislocation in Ti2AlC-MAX phase induced by matrix-Cu diffusion. Scripta Mater. 2021;191:34–9.
4. Huang X, Feng Y, Qian G, Zhao H, Zhang J, Zhang X. Physical, mechanical, and ablation properties of Cu–$Ti_3AlC_2$ composites with various $Ti_3AlC_2$ contents. Mater Sci Technol. 2018;34(6):757–62.
5. Sun Z. Progress in research and development on MAX phases: a family of layered ternary compounds. Int Mater Rev. 2011;56(3):143–66.
6. Low I-M. MAX phases and ultra-high temperature ceramics for extreme environments: IGI Global; 2013.
7. Salvo C, Chicardi E, Hernández-Saz J, Aguilar C, Gnanaprakasam P, Mangalaraja R. Microstructure, electrical and mechanical properties of Ti2AlN MAX phase reinforced copper matrix composites processed by hot pressing. Mater Charact. 2021;171: 110812.
8. Solodkyi I, Bezdorozhev O, Loboda P. High electrical conductive copper matrix composites reinforced with LaB6–TiB2 eutectic particles. Vacuum. 2020;177: 109407.
9. Jamwal A, Mittal P, Agrawal R, Gupta S, Kumar D, Sadasivuni KK, et al. Towards sustainable copper matrix composites: manufacturing routes with structural, mechanical, electrical and corrosion behaviour. J Compos Mater. 2020;54(19):2635–49.
10. Gelaw M, Ramulu PJ, Hailu D, Desta T. Manufacturing and mechanical characterization of square bar made of aluminium scraps through friction stir back extrusion process. Journal of Engineering, Design and Technology. 2018;16(4):596–615.
11. Mathew N, Dinaharan I, Vijay S, Murugan N. Microstructure and mechanical characterization of aluminum seamless tubes produced by friction stir back extrusion. Trans Indian Inst Met. 2016;69(10):1811–8.
12. Buffa G, Campanella D, Micari F, Fratini L. Design and development of a new machine tool for continuous friction stir extrusion. CIRP J Manuf Sci Technol. 2023;41:391–400.
13. Yuan L, Zeng X, Zhao X, Xie Y, Gandra J, Guan D. Microstructure evolution and tensile behaviour of fine-grained 6082 Al wire with high ultimate strength and high work hardening by friction stir extrusion of bulk Al sheet. Mater Sci Eng A. 2023;2023:144589.
14. Li X, Zhou C, Overman N, Ma X, Canfield N, Kappagantula K, et al. Copper carbon composite wire with a uniform carbon dispersion made by friction extrusion. J Manuf Process. 2021;65:397–406.
15. Jahani A, Jamshidi Aval H, Rajabi M, Jamaati R. Effects of Ti2SnC MAX phase reinforcement content on the properties of copper matrix composite produced by friction stir back extrusion process. Mater Chem Phys. 2023;299: 127497.
16. Akbari M, Asadi P. Brass wire forming by friction stir back extrusion: numerical modeling and experiment. 2021.
17. Jahani A, Jamshidi Aval H, Rajabi M, Jamaati R. Effects of Ti2SnC MAX phase on microstructure, mechanical, electrical, and wear properties of stir-extruded copper matrix composite. Adv Eng Mater. 2023;25:2201463.
18. Sabbaghian M, Shamanian M, Akramifard H, Esmailzadeh M. Effect of friction stir processing on the microstructure and mechanical properties of Cu–TiC composite. Ceram Int. 2014;40(8):12969–76.
19. Akbari M, Asadi P. Optimization of microstructural and mechanical properties of brass wire produced by friction stir extrusion using Taguchi method. Proc Inst Mech Eng Part L J Mater Des Appl. 2021;235(12):2709–19.
20. Dickson M. The significance of texture parameters in phase analysis by X-ray diffraction. J Appl Crystallogr. 1969;2(4):176–80.
21. Barmouz M, Givi MKB. Fabrication of in situ Cu/SiC composites using multi-pass friction stir processing: evaluation of microstructural, porosity, mechanical and electrical behavior. Compos A Appl Sci Manuf. 2011;42(10):1445–53.
22. Zohoor M, Givi MB, Salami P. Effect of processing parameters on fabrication of Al–Mg/Cu composites via friction stir processing. Mater Des. 2012;39:358–65.
23. Bahador A, Umeda J, Hamzah E, Yusof F, Li X, Kondoh K. Synergistic strengthening mechanisms of copper matrix composites with $TiO_2$ nanoparticles. Mater Sci Eng A. 2020;772: 138797.
24. Dinaharan I, Saravanakumar S, Kalaiselvan K, Gopalakrishnan S. Microstructure and sliding wear characterization of Cu/$TiB_2$ copper matrix composites fabricated via friction stir processing. J Asian Ceram Soc. 2017;5(3):295–303.
25. Wei J, Li Z, Han F. Thermal mismatch dislocations in macroscopic graphite particle-reinforced metal matrix composites studied by internal friction. Physica Status Solidi (A). 2002;191(1):125–36.